論文 / 著書情報
Article / Book Information

論題(和文)	Study of Co-deposition Photoelectrode of Perylene Derivative and Phthalocyanine in Comparison with Its Bilayer Focusing on Charge Transfer Complex and Kinetic Analysis
Title(English)	Study of Co-deposition Photoelectrode of Perylene Derivative and Phthalocyanine in Comparison with Its Bilayer Focusing on Charge Transfer Complex and Kinetic Analysis
著者(和文)	Mohd Fairus Bin Ahmad, 阿部敏之, Christopher S A Musgrave, 長井圭治
Authors(English)	Mohd Fairus Bin Ahmad, Toshiyuki Abe, Christopher S A Musgrave, Keiji Nagai
出典(和文)	ELECTROCHEMISTRY, Vol. 86, No. 5, pp. 235-242
Citation(English)	ELECTROCHEMISTRY, Vol. 86, No. 5, pp. 235-242
発行日 / Pub. date	2018, 9

Advance Publication by J-STAGE

Electrochemistry

The Electrochemical Society of Japan

Received: December 28, 2017
Accepted: April 24, 2018
Published online: June 1, 2018

https://doi.org/10.5796/electrochemistry.18-00001

Article

Electrochemistry, (in press)

Study of Co-deposition Photoelectrode of Perylene Derivative and Phthalocyanine in Comparison with Its Bilayer Focusing on Charge Transfer Complex and Kinetic Analysis

Mohd Fairus AHMAD,[a,b] Toshiyuki ABE,[c] Christopher S. A. MUSGRAVE,[a] and Keiji NAGAI[a,*]

[a] *Laboratory for Chemistry and Life Science, Institute of Innovative Research, Tokyo Institute of Technology, R1-26, Suzukake-dai, Midori-ku, Yokohama 226-8503, Kanagawa, Japan*
[b] *School of Microelectronic Engineering, Kampus Pauh, Universiti Malaysia Perlis, 02600, Arau, Perlis, Malaysia*
[c] *Department of Frontier Materials Chemistry, Graduate School of Science and Technology, Hirosaki University, 3 Bunkyo-cho, Hirosaki 036-8561, Japan*

* *Corresponding author: nagai.k.ae@m.titech.ac.jp*

ABSTRACT

The characteristics for 3,4,9,10-perylenetetracarboxylic-bisbenzimidazole (PTCBI, an n-type semiconductor) and 29H,31H-phthalocyanine (H_2Pc, a p-type semiconductor) as organic p/n bilayer and bulk heterojunction (BHJ) photoelectrodes were studied for the photooxidation of thiol. Based on the analysis in their absorption spectra, a new absorption band in the longer wavelength ($\lambda > 800$ nm) for both bilayer and co-deposited photoelectrode suggested a formation of charge transfer complex. A photoanodic current was observed at $\lambda \sim 880$ nm for the both bilayer and co-deposited electrodes, while no absorption and photocurrent for single layers of PTCBI and H_2Pc. By assuming the Langmuir adsorption equilibrium at the solid/water interface, the kinetic parameters for the photoanodic current of thiol was analyzed for the longer wavelength of irradiation ($\lambda \sim 900$ nm), and it was indicated that the rate of oxidation in the co-deposited was higher than that of the bilayer due efficient charge separation in the charge transfer complex.

Keywords : Organic Semiconductor, Heterojunction, Visible and Near Infrared Photocatalyst, Charge Transfer Complex

1. Introduction

High efficiency is required for the solar energy conversion devices to utilize full spectrum of solar light and quantum yield. Organic semiconductor (OSM) has interesting features such as wide spectrum of light absorption, low cost, simple fabrication process, and light weight. Stable organic semiconductor composed of p/n junction responsive to whole visible light was operated and utilized not only for photovoltaic (OPV),[1–10] but also photocatalyst.[11–20]

For the design of efficient OSM photocatalyst, material selection for p-type and n-type is different from photovoltaic devices. In the case of photocatalyst, p-type is oxidation part and phthalocyanine (Pc) exhibited as a co-catalyst site. It means conventional organic p-type semiconductor in photovoltaics typically has a role of light absorber such as P3HT which does not work as photocatalyst.[11] Then, n-type also required light absorption with much wider spectrum in OSM photocatalyst. In the sense, fullerene and PCBM are not good choice because of absorption only in the shorter wavelength region. Then, to construct an efficient photocatalyst, phthalocyanine and 3,4,9,10-perylenetetracarboxylic bisbenzimidazole (PTCBI) would be good candidate.

The combination was the first example of p/n junction organic photovoltaics[1] and has studied in terms of derivative change,[6–8] mechanism study,[8,9] bulk heterojunction study[21,22] etc. The bulk heterojunction is effective for the combination also.[22] For the case of the combination of phthalocyanine and PTCBI, bulk heterojunction (BHJ) structure was synthesized by co-deposition technique and exhibited an efficient charge separation due to the large area of donor-acceptor interface especially with the small light intensity.[21–23]

Unless the photovoltaics, in the past studies of p/n OSM photocatalyst, photoinduced charge separation was the rate determining step for only a high concentration of the substance of the reaction, while the electron transfer at solid/water interface was that for the low concentration.[24–27] Then the charge transfer complex formation is interesting not only for light absorption spectrum, but also kinetics of charge separation-recombination balance to correct redox process in photocatalyst. This paper focusses two aspects of light absorption and kinetics from the viewpoint of p/n interface in comparison of co-deposited sample and bilayer sample. Furthermore, donor/acceptor OSM interface can imply charge transfer complex of which interesting interaction happens between donor and acceptor[28,29] and can enhance the absorption of the system especially in the longer wavelength reaching to near infrared.[30–32] It will be great merits to utilize natural sun light efficiently. Since the bulk heterojunction photocatalyst is less studied than the bilayer p/n junction photocatalyst, then, it would be important to compare their contribution of charge transfer complex towards the photocurrent generation and to compare their kinetic parameters of photocatalysis at solid/water interface.

In this paper, we investigate the absorption and photocurrent for the photoelectrochemical thiol oxidation for the bilayer and co-deposited layer electrodes composed of metal-free Pc (H_2Pc) and PTCBI having electrode-electrolyte interface. From the absorption and photocurrent, the charge transfer complex and the kinetics of the photooxidation of thiol were discussed for both systems.

2. Experimental Condition

2.1 Materials

ITO glasses (sheet resistance = 10 Ω/cm^2; transmittance > 85%; ITO thickness = 174 nm; Asahi Glass Co., Ltd.) were cut into 2 cm × 1 cm size and cleaned using ultrasonication with acetone and

ethanol subsequently. PTCBI was synthesized[33] and purified by sublimation process. H_2Pc (Tokyo Chemical Industry Co., Ltd.) is commercially available and purified by sublimation prior to use. The sublimation of each PTCBI and H_2Pc was done in the tubular furnace (ATF350-AST3), custom made by Alpha Giken Co. 2-mercaptoethanol (Tokyo Chemical Industry Co., Ltd.) is commercially available and used as received.

2.2 Preparation of bilayer PTCBI/H_2Pc film (ITO/PTCBI/H_2Pc)

The photoelectrode device of ITO/PTCBI/H_2Pc was prepared by vapor deposition based on the method in previous literature.[34] PTCBI of 28 nm thickness was first coated (deposition speed, 0.12 nm s^{-1}) on ITO. Subsequently, H_2Pc of 41 nm thickness was coated (deposition speed, 0.06 nm s^{-1}) on top of the PTCBI.

2.3 Preparation of bulk heterojunction PTCBI:H_2Pc film (ITO/PTCBI:H_2Pc-A)

The BHJ was prepared by vapor deposition system equipped with multi heater, then the simultaneous coating of two materials was possible. Firstly, the ITO substrate was block during pre-deposition in the vacuum chamber, while the vapor deposition rates for PTCBI (0.13 nm s^{-1}) and H_2Pc (0.05 nm s^{-1}) were controlled one by one. After that, the ITO substrate was unblocked, so that the BHJ film was fabricated for about 409 s of deposition time.

2.4 Characterization by AFM and FESEM

The topography was measured in ambient condition with an Asylum Cypher S atomic force microscopy (AFM). The non-contact mode cantilevers (OCML-AC240TM, Olympus) were used with typical resonant frequency and spring constant about 70 kHz and 2 N/m respectively. For FE-SEM observation of ITO/PTCBI:H_2Pc-A sample on cross section, the sample was cleaved, and the cross section was coated by sputtering Pt for 10 mA, 30 s by ion sputter coater (MC 1000, Hitachi). The cross-sectional image was obtained by high resolution scanning electron microscope (S-5500, Hitachi).

2.5 Electrochemistry measurement

The electrochemistry measurement was conducted in the cell that composed of the deposited electrode as working electrode. The working electrode was contacted with wire and DOTITE to ITO area and fastened by epoxy resin. The counter electrode and the reference electrode was Pt and Ag/AgCl respectively. The electrolyte was 2-mercaptoethanol (in KOH, pH 11) was stirred during the measurement. Halogen light source (Megalight 100, SCHOTT) was used to irradiate white light, at intensity of 70 mW/cm^2. Its spectrum is shown elsewhere.[14] Monochromator (SM-GTD, BUNKOUKEIKI Co., Ltd.) was used for the action spectrum photocurrent measurement, with controlled photon number $= 1 \times 10^{16}$ photons cm^{-2} s^{-1}.

3. Results and Discussion

3.1 Characterization by AFM and FESEM

Atomic force microscopy (AFM) was used to measure the surface's topography of monolayer PTCBI and H_2Pc, the bilayer ITO/PTCBI/H_2Pc and the co-deposited ITO/PTCBI:H_2Pc-A. As shown in Figs. 1a and b, the surface roughness of monolayer PTCBI was about 10 nm, while it was 20 nm for monolayer H_2Pc. The crystal size for each of them was about 200 nm. For the bilayer ITO/PTCBI/H_2Pc (Fig. 1c), the high-resolution scan (4 nm resolution scan) showed that the surface roughness and the crystal size were about 8 nm and 50 nm for lateral direction, respectively. For the co-deposited ITO/PTCBI:H_2Pc-A (Fig. 1d), by estimating from a 4 nm resolution scan, the particles size was not clearly observed and the roughness was <8 nm level. It was much smaller than that the cases of monolayer and the phase separation between the PTCBI and H_2Pc was not clearly observed in the image. The tendency is similar to the

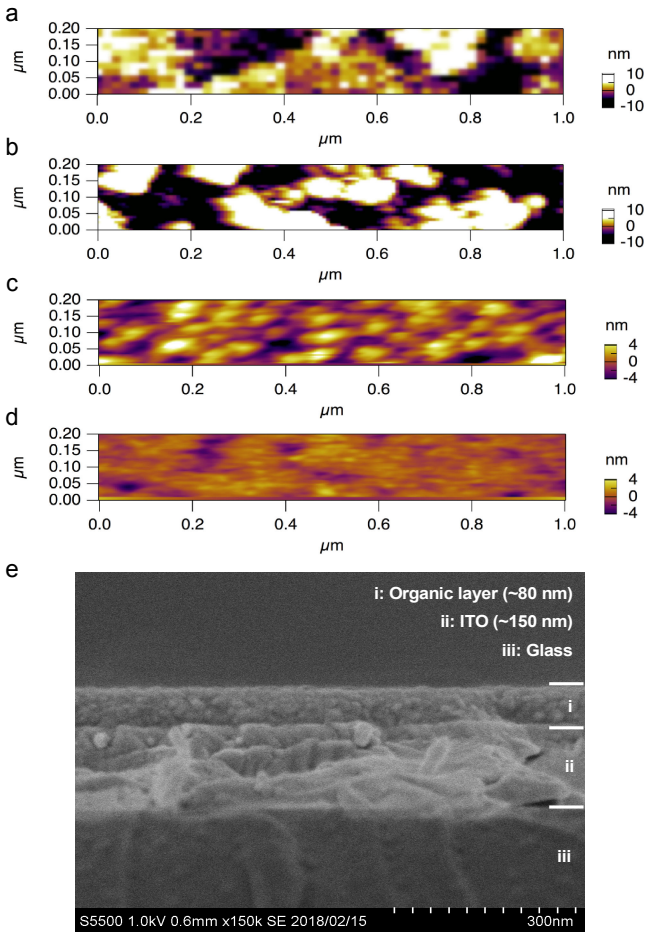

Figure 1. Topography images for monolayer PTCBI (a), monolayer H_2Pc (b), bilayer ITO/PTCBI/H_2Pc (c) and co-deposited ITO/PTCBI:H_2Pc-A (d). The space resolution of the scan is 19 nm for (a), 8 nm for (b) while 4 nm for (c, d). (e) FE-SEM image of cross sectional view of co-deposited electrode.

previous case of PTCBI and copper phthalocyanine (CuPc),[22] and it was simulated as single nanometer phase separation. The smoothness in the co-deposited ITO/PTCBI:H_2Pc-A suggest the formation of bulk heterojunction structure.

To characterize more about the morphology of co-deposited ITO/PTCBI:H_2Pc-A sample, the sample was cleaved, and the cross section was observed by FE-SEM (Fig. 1e). The thickness of organic layer was ca. 80 nm on the 150 nm thickness of ITO layer. The surface roughness was ca. 5 nm, which is almost similar to that of the AFM topography measurement (Fig. 1d). The crystal size was <20 nm, suggesting the phase separation between PTCBI and H_2Pc occurred within the co-deposited layer. The phase separation was not clearly observed in the case of topography image (Fig. 1d), suggesting that the large particles (20 nm) are covered with the small particles (<20 nm) and thus correspond to the smoothness of the surface.

3.2 Visible light absorption

3.2.1 Comparison between monolayer and bilayer

Figure 2(a) shows the absorption spectrum for monolayers of PTCBI (Abs_{PTCBI}), H_2Pc (Abs_{H2Pc}), and bilayer of PTCBI/H_2Pc ($Abs_{bilayer}$). The monolayer PTCBI (purple solid line) showed broad in the visible region and has a peak at $\lambda = 540$ nm, and a shoulder reaching to infra-red region is lying at $\lambda \approx 800$ nm. The monolayer H_2Pc (blue solid line) has a peak in the visible region at $\lambda \approx 620$ nm. Both of them are identical to the previous reports[35] and using their absorbance-thickness coefficient value (PTCBI: 3.2×10^{-3} nm^{-1} at

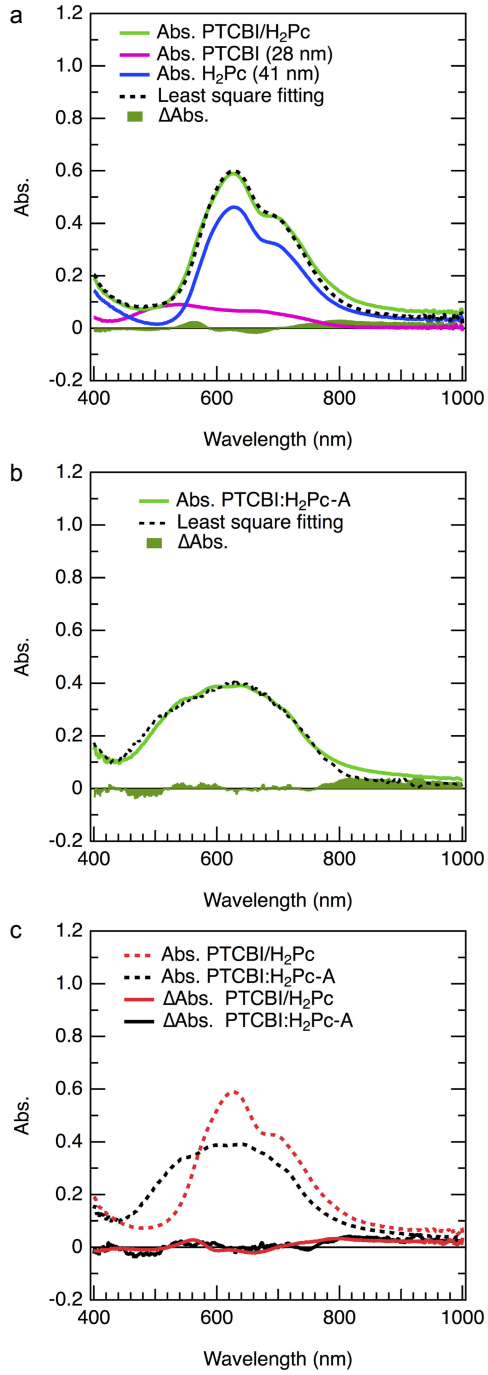

Figure 2. (a, b) Absorption spectrum (green solid line) and ΔAbs (shaded green area) for (a) PTCBI/H_2Pc and (b) PTCBI:H_2Pc-A. Absorption spectrum of monolayers PTCBI and H_2Pc are shown in (a) by the solid purple line and solid blue line, respectively. The least square fitting is shown in by the black dashed line. The thickness values for fiting the bilayer PTCBI/H_2Pc gives PTCBI = 24 nm, H_2Pc = 48 nm, while for fitting the co-deposited PTCBI:H_2Pc-A gives PTCBI = 82 nm, H_2Pc = 19 nm. The summary of absorbance spectrum (green solid line) and Δ*Abs* (shaded green area) for both electrodes in (a) and (b) is shown in (c).

λ = 540 nm, H_2Pc: 11×10^{-3} nm^{-1} at λ = 630 nm), the thickness values were estimated to be 28 nm for PTCBI and 41 nm for H_2Pc respectively. The bilayer PTCBI/H_2Pc (Fig. 2a, solid green line) looks like the sum of absorption of monolayers. By the least square fitting as equation below,

$$Abs_{fitting} = t_1 Abs_{PTCBI} + t_2 Abs_{H_2Pc} \quad (1)$$

the thickness of each monolayer was estimated to be 24 nm for PTCBI and 48 nm for H_2Pc, respectively and the spectrum is shown as dashed black line of Fig. 2a. It is noticed that there is a difference in near infra-red region between the fitting spectrum and bilayer spectrum. The difference of spectrums (Δ*Abs*) was estimated by the following equation,

$$\Delta Abs = Abs_{Bilayer\ or\ co\text{-}deposited} - Abs_{fitting} \quad (2)$$

The Δ*Abs* spectrum is shown in the Fig. 2a by the green shaded area. The threshold for longer wavelength region was at λ ≈ 700 nm and continues to near infra-red. This broad absorption could be indication for charge transfer complex formation.

There have been defined that charge transfer complex has an interaction between donor and acceptor molecules when a partial of electronic charge is transferred from the donor to the acceptor moiety.[29] Generally, charge transfer complex has binding energy correlated with the energy difference between highest occupied molecular orbital (HOMO) of the donor and the lowest unoccupied molecular orbital (LUMO) of the acceptor. The difference between the HOMO of H_2Pc (donor) and LUMO of PTCBI (acceptor) is >0.6 eV, which resembles λ < 2060 nm.

3.2.2 Comparison between monolayer and bulk heterojunction

Figure 2b shows the absorption spectrum for co-deposited PTCBI:H_2Pc-A ($Abs_{co\text{-}deposited}$). Here again, we tried least square fitting again by using Eq. (1) for the co-deposited layer as shown on dashed black line in Fig. 2b. The difference between the fitted value and original data was estimated by the Eq. (2), and shown as green shaded area in Fig. 2b. It has broad absorption at λ > 760 nm and suggesting charge transfer complex formation due to the same reason as described before. From the fitting, the thickness values for PTCBI and H_2Pc were 82 nm and 20 nm, respectively and the summation of them gives total thickness of 102 nm, which is >20% thicker than that observed by FE-SEM, 80 nm (Fig. 1e). One of the possible reason is the co-deposited layer has high density of PTCBI and H_2Pc molecules, but looks too high (>20%). Another possible reason is related to molecular orientation, in which the co-deposited layer might have random orientation (i.e. not planar orientation) and hence it had a high light absorbance.

3.2.3 Comparison between bilayer and bulk heterojunction

Both bilayer PTCBI/H_2Pc and co-deposited PTCBI:H_2Pc-A exhibited small absorption bands that are not shown in either of monolayer component. The Δ*Abs* spectra for both samples were summarized into Fig. 2c (solid lines). As shown in the Fig. 2c (Δ*Abs*, λ > 800 nm), both bilayer PTCBI/H_2Pc and co-deposited PTCBI:H_2Pc-A had similar positive value of Δ*Abs* at the longer wavelength.

3.3 I-V measurement and rest potential measurement

Figure 3 shows the cyclic voltammogram for the oxidation of 2-mercaptoethanol with ITO/PTCBI/H_2Pc (Fig. 3a) and ITO/PTCBI:H_2Pc-A (Fig. 3b) electrodes under the dark and halogen light irradiation. At +0.2 V vs. Ag/AgCl, the photoanodic current density of ITO/PTCBI/H_2Pc (Fig. 3a, red), and ITO/PTCBI:H_2Pc-A (Fig. 3b, red) was 90 and 45 μA/cm^2 respectively. Both electrode has similar photoanodic threshold voltage at −0.15 V vs. Ag/AgCl.

Table 1 shows the rest potential (open circuit potential) of the single layer electrodes, bilayer electrode and the co-deposited electrode for the measurement under the dark ($V_{R\text{-}dark}$) and illumination ($V_{R\text{-}light}$) condition. The rest potential values were identical to those of the previous paper; i.e., Monolayer ITO/PTCBI and ITO/H_2Pc have been exhibited typical p-type and n-type Schottky junction with electrolyte; i.e. photocathode and photo-anode, respectively.[14] The bilayer ITO/PTCBI/H_2Pc had similar polarity to ITO/PTCBI, and its tendency was the same as reported earlier. The co-deposited ITO/PTCBI:H_2Pc-A also had similar polarity to ITO/PTCBI and implies possibility for the existence of PTCBI/water interface.

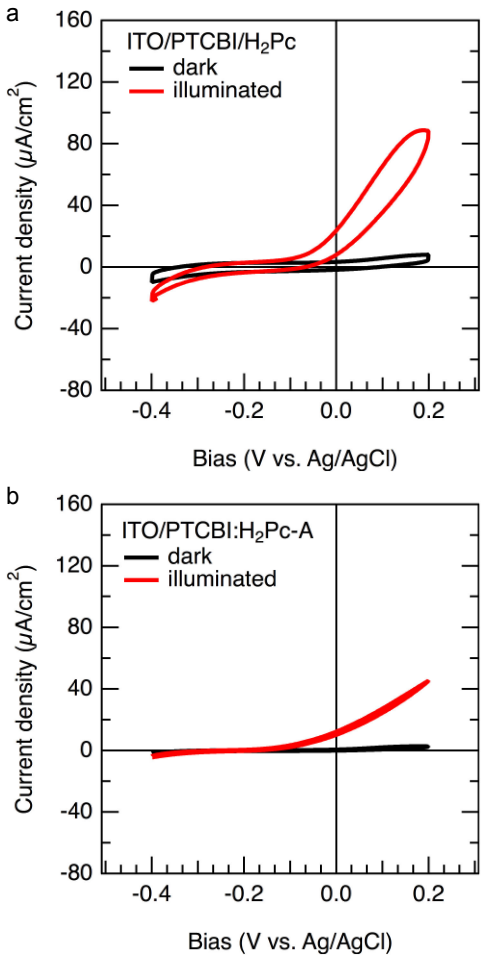

Figure 3. CV for the ITO/PTCBI/H_2Pc (a) and ITO/PTCBI:H_2Pc-A (b) electrodes under the dark (black) and illumination (red) conditions. The electrochemical cell was consisted of reference electrode: Ag/AgCl, counter electrode: Pt and electrolyte: 10 mmol dm^{-3} of 2-mercaptoethanol in KOH (pH 11). The irradiation condition: halogen light, 70 mW/cm^2; irradiation side, ITO. Scan rate: 20 mV/cm^2.

Table 1. Rest potential (V_R) for bilayer and co-deposited electrodes under dark ($V_{R\text{-dark}}$) and under illumination ($V_{R\text{-light}}$).

ITO/(layer)	$V_{R\text{-dark}}$ (V)	$V_{R\text{-light}}$ (V)	$V_{R\text{-light}} - V_{R\text{-dark}}$ (V)
PTCBI (50 nm)	−0.14	−0.22	−0.08
H_2Pc (50 nm)	−0.17	+0.23	+0.40
PTCBI (28 nm)/H_2Pc (41 nm)	−0.19	−0.22	−0.03
PTCBI:H_2Pc-A (72 nm)	−0.16	−0.19	−0.04

Electrochemical cell was consisted of reference electrode: Ag/AgCl, counter electrode: Pt and electrolyte: 10 mmol dm^{-3} of 2-mercaptoethanol in KOH (pH 11). The irradiation condition: halogen light, 70 mW/cm^2; irradiation side, ITO. Error in the voltage fluctuation: ±0.001 V.

3.4 Action spectrum photocurrent in for constant thiol concentration

To investigate the origin of the photocurrent, its action spectrum was obtained with the thiol concentration = 10 mmol dm^{-3}. Figure 4(a) are for the bilayer ITO/PTCBI/H_2Pc for the irradiation from the ITO side. For the irradiation from the ITO side, the photocurrent density was corresponded to the absorption spectrum, and it peaked at the irradiation of λ = 540 nm. It shows that photocurrent for the fabricated bilayer was efficient at the high absorbance in PTCBI. By comparing data in Figs. S1a and b of the Supporting Information (SI), the photocurrent density was almost corresponded to the absorption spectrum, where the photocurrent density was highest at the irradiation of λ = 540 nm instead of at λ = 590 nm.

The difference above is a typical phenomenon, ascribed as filter effect by H_2Pc layer in the ITO/PTCBI/H_2Pc electrode, previously.[27,36,37] In those studies, the filter effect was occurred at the irradiation from the H_2Pc side, where the action spectrum was good agreement with the transmittance spectrum of H_2Pc. The interpretation was that the exciton in H_2Pc was quenched by electrolyte, while photovoltaic system of the bilayer exhibited the contribution of H_2Pc absorption due to the absence of electrolyte.

Figure 4(b) show the photocurrent density of the ITO/PTCBI:H_2Pc-A. As shown in Figs. S1c and d, the trend of the action spectrum for both irradiation sides was corresponded to the absorption spectrum of ITO/PTCBI:H_2Pc-A. The similarity not to depend on the illumination side suggests small exposure of H_2Pc to electrolyte due to BHJ structure.

The internal quantum efficiency (IQE) was calculated by the following equation (Eq. (3)) below

$$\text{IQE}\ (\%) = \{[J/e]/[\text{photon flux}\ (1 - 10^{-Abs})]\} \times 100 \quad (3)$$

where J (A/cm^2) is the photocurrent density, and e (C) is the elementary charge. The peak shift from the current density for bilayer is due to the filter effect as described before, while the shift did not happen for co-deposited electrode. The IQE (%) values for the co-deposited electrode in entire wavelength were smaller than that of the case of bilayer ITO/PTCBI/H_2Pc, suggesting a relation to higher recombination event than that of the bilayer PTCBI/H_2Pc, maybe due to high charge separation efficiency of BHJ. The possible processes are summarized in Table 2 and the recombination process whose rate is as below (Eq. (4))

$$R = \frac{q(\mu_e + \mu_h)}{\varepsilon}(np) \quad (4)$$

where n, p are the density of photogenerated electron (in conduction band) and hole (in valence band), μ_e, μ_h are the electron and hole mobilities, and ε is dielectric permittivity. Because there are more p/n junctions area in the BHJ than that for bilayer, then more charge separation and non-geminate recombination is expected. Moreover, the geminate recombination for exciton could also occur due to the larger particle size (Fig. 1e, ~12–20 nm) than the exciton diffusion length for PTCBI (3–5 nm) and H_2Pc (7–12 nm).[38]

The contribution of charge transfer complex towards the generation of photocurrent can be investigated in the action spectrum data at the longer wavelength, λ > 800 nm by comparing the action spectrum for monolayer electrode with that of the bilayer and co-deposited electrodes. The experiment for action spectrum of photocurrent density in monolayer electrode ITO/PTCBI (50 nm) and ITO/H_2Pc (50 nm) was conducted, as shown in Fig. 5a. The photocurrent value for monolayer electrode ITO/PTCBI (50 nm) was <0.4 μA/cm^2 and showed threshold for photocurrent at λ ≈ 860 nm, while almost no photocurrent for ITO/H_2Pc (50 nm) for λ > 800 nm.

As shown in Fig. 5(b) the photocurrent was exhibited in ITO/PTCBI/H_2Pc at λ > 800 nm and was in agreement with their Δ*Abs* spectrum. The photocurrent generation was exhibited at λ > 860 nm, demonstrated that much longer wavelength can generate photocurrent than that of the monolayer electrodes even though the PTCBI thickness in the bilayer was about half than that in the case of monolayer ITO/PTCBI electrode. This shows that the generation of photocurrent at λ > 860 nm for the bilayer did not depend on the PTCBI thickness. As shown in Fig. 5(c), photocurrent density was

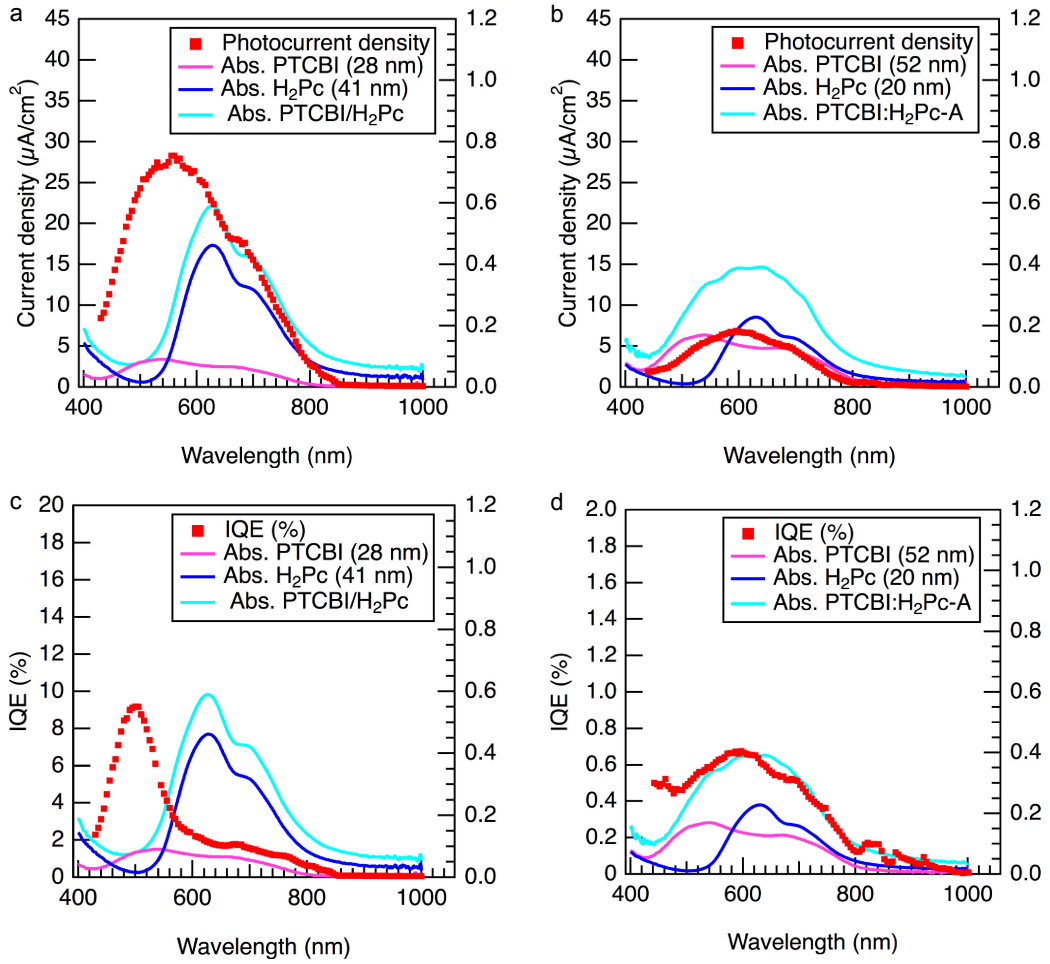

Figure 4. (a, b) Action spectra and (c, d) IQE (%) for photocurrent density for ITO/PTCBI/H_2Pc (a, c), and ITO/PTCBI:H_2Pc-A (b, d) with 5 nm resolution of scan. Photon flux: 1.0×10^{16} photons cm^{-2} s^{-1}. Electrolyte: 10 mmol dm^{-3} of 2-mercaptoethanol in KOH (pH 11) under stirring. Bias; 0.2 V vs. Ag/AgCl.

Table 2. Element processes for the photoanodic current generation and recombination.

Process	Reaction		Product
Light absorption	PTCBI + hν	→	PTCBI*
Light absorption	H_2Pc + hν	→	H_2Pc*
Exciton diffusion	(PTCBI* + PTCBI)	→	PTCBI + PTCBI*
Exciton diffusion	(H_2Pc* + H_2Pc)	→	H_2Pc + H_2Pc*
Exciton diffusion to the p/n junction	PTCBI* + (PTCBI-H_2Pc)	→	PTCBI + (PTCBI-H_2Pc)*
Exciton diffusion to the p/n junction	H_2Pc* + (PTCBI-H_2Pc)	→	H_2Pc + (PTCBI-H_2Pc)*
Charge separation	(PTCBI-H_2Pc)*	→	($PTCBI^-$-H_2Pc^+)
Conduction	$H_2Pc^+_{(bulk)}$ + $H_2Pc_{(surface)}$	→	$H_2Pc_{(bulk)}$ + $H_2Pc^+_{(surface)}$
Non-geminate recombination	$PTCBI^-_{(interface)}$ + $H_2Pc^+_{(interface)}$	→	PTCBI + H_2Pc
Geminate recombination	PTCBI*	→	PTCBI
Geminate recombination	H_2Pc*	→	H_2Pc

$[H_2Pc^+_{(surface)}] = [h^+]_0$.

also exhibited in ITO/PTCBI:H_2Pc-A at $\lambda > 860$ nm. The threshold for the photocurrent generation in the co-deposited electrode was at $\lambda = 980$ nm, while in the bilayer was at $\lambda = 940$ nm. The generation of photocurrent in ITO/PTCBI/H_2Pc and ITO/PTCBI:H_2Pc-A would be originated from the light absorption by the charge transfer complex at $\lambda > 800$ nm region. The more photocurrent at $\lambda > 940$ nm for the co-deposited one than that for bilayer also agrees with charge transfer complex contribution because co-deposited electrode has more H_2Pc/PTCBI interface.

3.5 Photoanodic current and its analysis

We conducted thiol concentration dependent current measurement. For the light on-off experiment, under illumination, initially a spiky photocurrent (J_{in}) was observed, and it then attains a steady-state photocurrent (J_s) as shown in Fig. S2 of SI. Figure 6(a, open circles) shows the spiky and steady state photocurrents density for bilayer ITO/PTCBI/H_2Pc. The effective photocurrent density was saturated at the increasing thiol concentration at 5 mmol dm^{-3} which is similar to the case of the dark current. For such on-off current, a

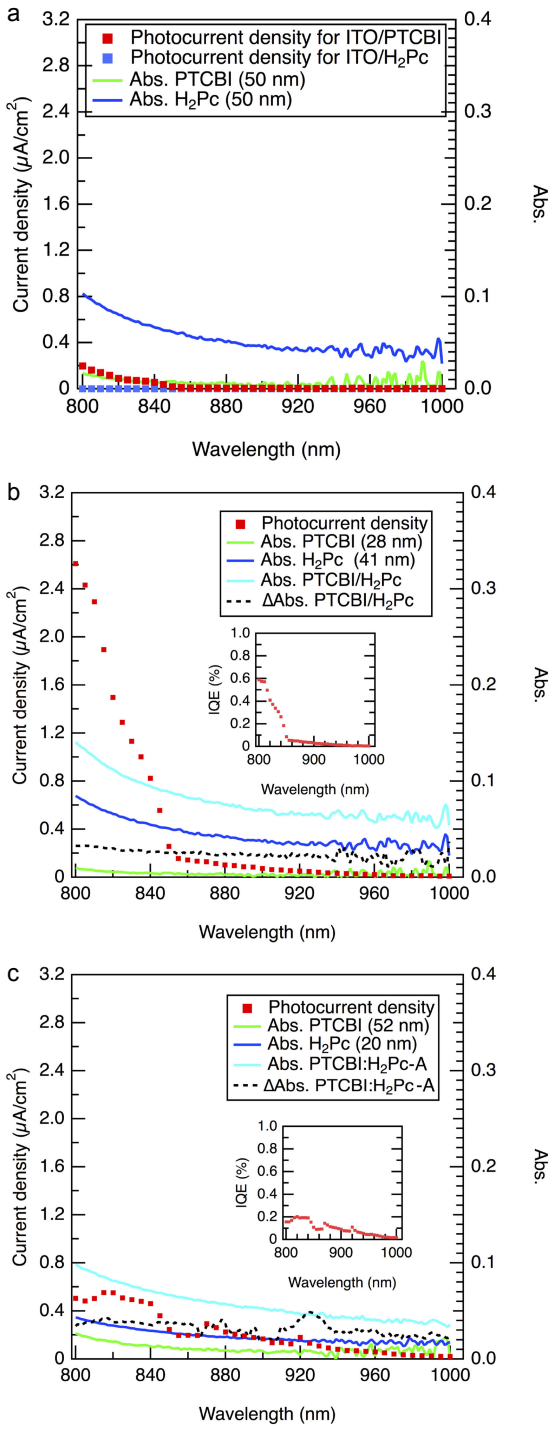

Figure 5. Action spectra for effective photocurrent density (i.e. dark current value subtract from photocurrent value) for (a) single layer ITO/PTCBI and ITO/H_2Pc, (b) ITO/PTCBI/H_2Pc, and (c) ITO/PTCBI:H_2Pc-A for $\lambda > 800$ nm. Inset of (b) and (c) shows IQE (%) data. Photon flux: 1.0×10^{16} photons cm^{-2} s^{-1}. Electrolyte: 10 mmol dm^{-3} of 2-mercaptoethanol in KOH (pH 11) under stirring. Bias; 0.2 V vs. Ag/AgCl. Error (or fluctuation) for current density measurement: ± 0.005 μA/cm^2.

mechanism has been proposed as shown in Fig. 7.[27] There, Langmuir adsorption equilibrium was assumed, and adsorption step of thiol is slower than that hole transfer at the solid/water interface.[27] It was also assumed only absorbed species oxidized and that the reduction product desorb quickly, and the photocurrent density J shows the first order dependence on the surface concentrations of the photogenerated hole, $[h^+]_0$ and the adsorbed thiol, Γ.[39]

$$J/nF = k_f[h^+]_0\Gamma \tag{5}$$

where, n is the number of electrons transferred from a thiol molecule to H_2Pc; F, Faraday's constant; and k_f, rate constant of the electron transfer.

If Langmuir adsorption equilibrium is assumed for thiol, the following equation is valid:

$$d\Gamma/dt = k(\Gamma_{max} - \Gamma) - k'\Gamma - k_f[h^+]_0\Gamma \tag{6}$$

where k: rate constant of adsorption, k': rate constant of desorption, and Γ_{max}: maximum coverage arising from the occupation of all available sites. At initial stage under illumination, the J_{in}, is derived by assuming change in $[h^+]_0$ occur faster than that of Γ, and therefore it is similar to the dark value of Γ and thus gives, $d\Gamma/dt = 0$; $k_f[h^+]_0\Gamma = 0$; Rearranging the Eqs. (5) and (6), the following equation is obtained

$$\frac{C_R}{J_{in}} = \frac{C_R}{J_{max}} + \frac{k'/k}{J_{max}} \tag{7}$$

where J_{max} is correspond for hypothetical photocurrent for Γ_{max} and C_R: thiol concentration. At steady state under illumination, $k_f[h^+]_0\Gamma \neq 0$, thus the following equation is obtained:

$$\frac{C_R}{J_S} = \frac{C_R}{J_{max}} + \frac{\{(k'/k) + (k_f[h^+]_0\Gamma)\}}{J_{max}} \tag{8}$$

As shown in Table 3, the kinetic parameters for the bilayer ITO/PTCBI/H_2Pc were obtained based on the C_R/J vs. C_R plots as in Fig. 6(c) for the irradiation of $\lambda = 900$ nm. The significant difference in the slope of C_R/J vs. C_R plots between that of the spike and steady states, indicates the limit of the model.[39] Columns I and II give the values to the kinetic parameters of bilayer ITO/PTCBI/H_2Pc for the irradiation of $\lambda = 900$ nm, while column a and b give that of relative values. The calculated J_{max} values were almost similar to the saturation value of the effective photoanodic current at $C_R > 5$ mmol dm^{-3}. K ($= 4.36 \times 10^3$ (mol dm^{-3})$^{-1}$) and $k_f[h^*]_0/k$ ($= 9.09 \times 10^{-5}$ mol dm^{-3}) can be interpreted as the effectiveness of adsorption of thiol and oxidation reaction, respectively. Occasionally these values were within the same order as the case of zinc(II)octacyanophthalocyanine single layer ($K = 7.1 \times 10^4$ (mol dm^{-3})$^{-1}$, $k_f[h^*]_0/k = 4.8 \times 10^{-4}$ mol dm^{-3}).[39]

For the co-deposited ITO/PTCBI:H_2Pc-A, we have tried the same analysis (Fig. 6d–f) as in the bilayer case. The obtained kinetic parameters are shown (Table 3). From here we compared the kinetic parameters between the co-deposited and bilayer electrodes. The J_{max} difference is reasonably interpreted as the difference of photogenerated hole carrier by the charge transfer complex; i.e. the co-deposited electrode may have higher charge transfer complex formation than that of the bilayer. There are three other important information about the analyzed data. The first is the same-order of K value, would be due to the same saturation of the adsorption at $C_R > 5$ mmol dm^{-3}. The second is large difference of $k_f[h^+]_0/k$ value between the co-deposited (1.62×10^{-3} mol dm^{-3}) and bilayer (9.09×10^{-5} mol dm^{-3}) electrodes. Since the K ($= k'/k$) values were similar, we may expect the similar k values for both the bilayer and the co-deposited electrode and then larger $k_f[h^+]_0$ for the co-deposited electrode. The third is the difference between the $k_f[h^+]_0/k'/I$ values. This parameter is to normalize the efficiency of oxidation by the light absorption (I). Then, the one-order high of $k_f[h^+]_0/k'/I$ value for the co-deposited electrode, indicates much larger oxidation rate for the co-deposited electrode than that of the bilayer.

We also compare the above kinetic parameters with that of case of shorter wavelength, $\lambda = 600$ nm (Table S1 of SI). It was found that the $k_f[h^+]_0/k'/I$ values (i.e. b values) for the bilayer electrode was the same order irrespective the wavelength ($b = 2.38$) employed and resembles the similarity in the efficiency to generate $[h^+]_0$ by the light absorption. Moreover, the K values were the

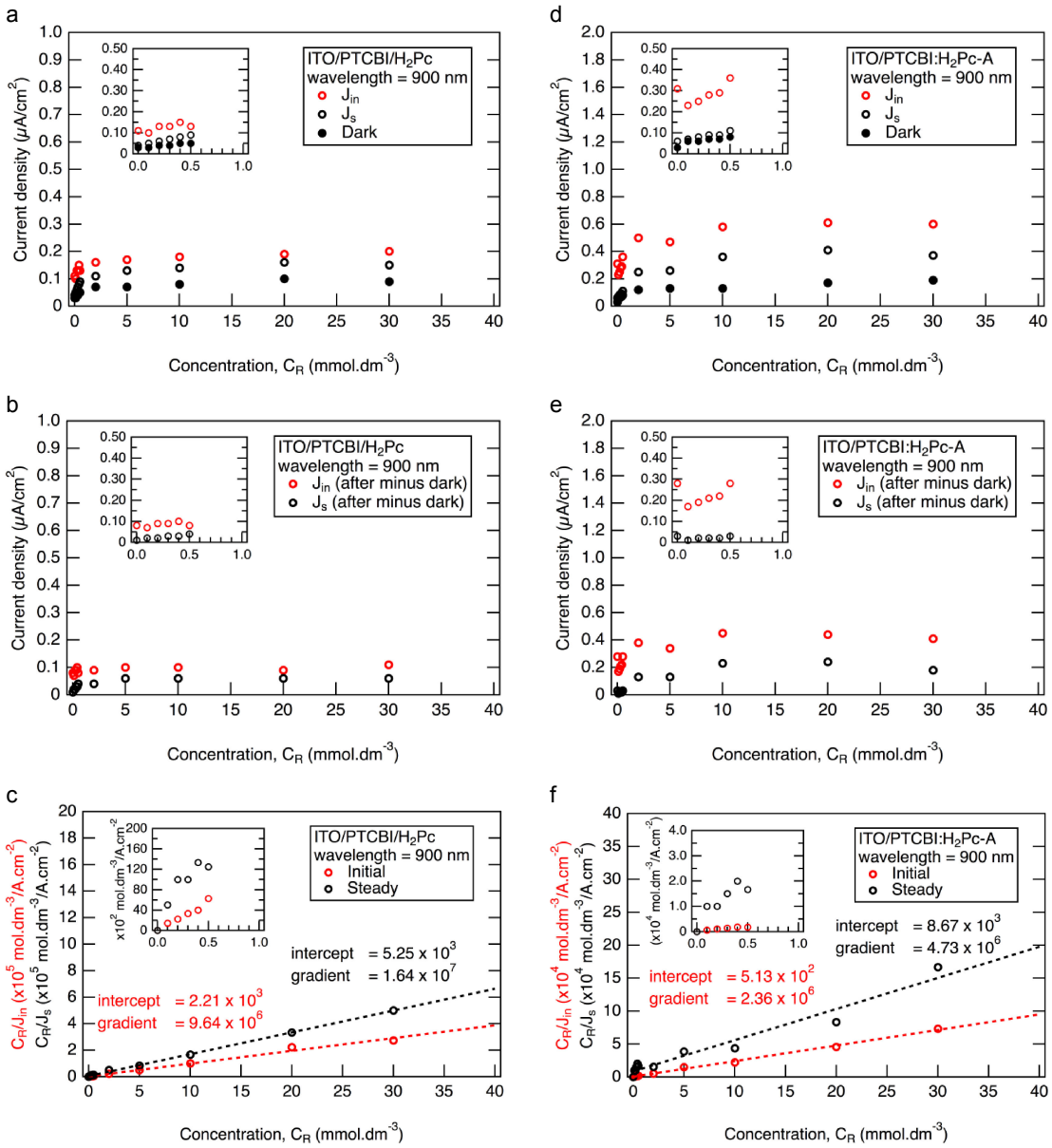

Figure 6. (a, d) Current density for the dark (filled black circle) and under illumination for spike (unfilled red circle) and steady (unfilled black circle) photocurrent density for (a) ITO/PTCBI/H_2Pc and (d) ITO/PTCBI:H_2Pc-A. (b, e) Effective photocurrent density (i.e. after the dark current density) was subtracted from the photocurrent density for ITO/PTCBI/H_2Pc (b) and ITO/PTCBI:H_2Pc-A (e). (c, f) C_R/J vs. C_R plots for ITO/PTCBI/H_2Pc (c) and ITO/PTCBI:H_2Pc-A (f). Electrolyte: 2-mercaptoethanol in KOH (pH 11). Applied bias: +0.2 vs. Ag/AgCl. Irradiation condition: $\lambda = 900$ nm, photon flux $= 1.0 \times 10^{16}$ photons $cm^{-2}\,s^{-1}$ (Light intensity $= 2.2$ mW/cm^2) and the side of irradiation was from the ITO side. $Abs_{Bilayer} = 0.069$, $Abs_{co\text{-}deposited} = 0.052$. From Lambert Beer law, Absorption (I) $= (1 - 10^{-Abs}/1) \times 100$, then I for bilayer $= 14.7\%$, while for co-deposited layer $= 11.2\%$.

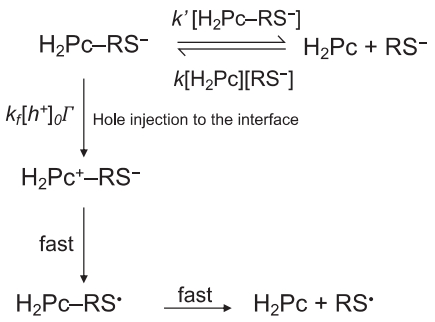

Figure 7. Mechanism of thiol photooxidized at H_2Pc/water interface for the ITO/PTCBI/H_2Pc. RS^- = thiol anion. k: rate constant of adsorption, k': rate constant of desorption, k_f, rate constant of the electron transfer. Modified from Ref. 27.

same order (i.e. $a = 1.0$–2.5) for both electrodes irrespective to the wavelength employed except for the case of $\lambda = 600$ nm, the co-deposited electrode has two-order lower (i.e. $a = 0.03$). Obviously, the electrolyte solution/H_2Pc interface area is small for the co-deposited film and orientation would affect the binding constant (K). Therefore, the low K (i.e. a) value of the co-deposited electrode in the case of $\lambda = 600$ nm might be related to direct photooxidation of adsorbed thiol on PTCBI site through exciton, while in the case of $\lambda = 900$ nm, the thiol might not be photooxidized on PTCBI site but on the PTCBI/H_2Pc junction site through the charge transfer complex, and thus the binding constant K might be different for both sites. On the other hand, the efficiency of photooxidation based on the $k_f[h^+]_0/k'/I$ values (i.e. b values) for the co-deposited electrode was one order lower ($b = 0.15$) than that of the bilayer ($b = 2.38$). It might be related to the exciton generated in the PTCBI is not efficiently quenched by the H_2Pc to generate holes. The overall

Table 3. Resulting kinetic parameter in ITO/PTCBI/H_2Pc and ITO/PTCBI:H_2Pc-A and the relative kinetic parameter in ITO/PTCBI:H_2Pc-A to ITO/PTCBI/H_2Pc for irradiation condition: $\lambda = 900$ nm.

	Jmax from J_{in} ($\mu A \cdot cm^{-2}$)	*Jmax* from J_s ($\mu A \cdot cm^{-2}$)	k'/k	K (I)	*relative rate with K*, (*a*)	$k_f[h^+]_0/k$ (II)	$k_f[h^+]_0/k'$ (I × II)	$(k_f[h^+]_0/k')/I$	*relative rate with* $(k_f[h^+]_0/k')/I$, (*b*)
			(mol dm^{-3})	(mol dm^{-3})$^{-1}$		(mol dm^{-3})			
ITO/PTCBI/H_2Pc	0.10	0.06	2.29×10^{-4}	4.36×10^{3}	1.00	9.09×10^{-5}	4.00×10^{-1}	3.00×10^{-2}	1.00
ITO/PTCBI:H_2Pc-A	0.42	0.21	2.17×10^{-4}	4.60×10^{3}	1.05	1.62×10^{-3}	7.45×10^{0}	6.70×10^{-1}	22.33

The kinetic parameter in ITO/PTCBI/H_2Pc and ITO/PTCBI:H_2Pc-A was obtained from the data of Fig. 6(c and e) by using Eq. (7) and (8). Irradiation condition: $\lambda = 900$ nm, photon flux $= 1.0 \times 10^{16}$ photons cm^{-2} s^{-1} (Light intensity $= 2.2$ mW/cm^2) and the side of irradiation was from the ITO side. The inverse of k'/k $(= k/k' = K)$ represents the equilibrium constant for thiol adsorption. $Abs_{Bilayer} = 0.069$, $Abs_{co\text{-}deposited} = 0.052$. From Lambert Beer law, Absorption $(I) = (1 - 10^{-Abs}/1) \times 100$, then I for bilayer $= 14.7\%$, while for co-deposited layer $= 11.2\%$. *a* and *b* are respectively the relative K value and $k_f[h^+]_0/k'/I$ value in each system and the value for ITO/PTCBI/H_2Pc is unity.

kinetics study shows that the co-deposited electrode is more efficient than that of the bilayer electrode for utilizing light in the longer wavelength, where the efficiency of photooxidation rate indicates the efficiency of charge separation in the charge transfer complex in the bulk heterojunction structure.

4. Conclusion

For both of bilayer and co-deposited electrode, light absorption at $\lambda > 800$ nm was observed as difference from the sum of monolayers, and photoanodic current also observed for both bilayer and co-deposited electrode for $\lambda > 800$ nm. Such longer wavelength absorption and photocurrent would be attributed to charge transfer complex at PTCBI/H_2Pc interface.

On the kinetic aspects of photoanodic current for thiol oxidation, the high efficiency for thiol oxidation in ITO/PTCBI:H_2Pc-A than that of in ITO/PTCBI/H_2Pc was observed under irradiation of longer wavelength and would be due to the efficient charge separation in the charge transfer complex in the bulk heterojunction structure.

Supporting Information

The Supporting Information is available on the website at DOI: https://doi.org/10.5796/electrochemistry.18-00001.

References

1. C. W. Tang, *Appl. Phys. Lett.*, **48**, 183 (1986).
2. S. M. Menke and R. J. Holmes, *Energy Environ. Sci.*, **7**, 499 (2014).
3. C. J. Brabec, M. Heeney, I. McCulloch, and J. Nelson, *Chem. Soc. Rev.*, **40**, 1185 (2011).
4. A. Facchetti, *Chem. Mater.*, **23**, 733 (2011).
5. A. W. Hains, Z. Liang, M. A. Woodhouse, and B. A. Gregg, *Chem. Rev.*, **110**, 6689 (2010).
6. D. Wöhrle, L. Kreienhoop, G. Schnurpfeil, J. Elbe, B. Tennigkeit, S. Hiller, and D. Schlettwein, *J. Mater. Chem.*, **5**, 1819 (1995).
7. I. Hiromitsu, M. Kitano, R. Shinto, and T. Ito, *Solid State Commun.*, **113**, 165 (2000).
8. K. Murata, S. Ito, K. Takahashi, and B. M. Hoffman, *Appl. Phys. Lett.*, **68**, 427 (1996).
9. T. Osasa, Y. Matsui, T. Matsumura, and M. Matsumura, *Sol. Energy Mater. Sol. Cells*, **90**, 3136 (2006).
10. D. Schlettwein and N. R. Armstrong, *J. Phys. Chem.*, **98**, 11771 (1994).
11. T. Abe, M. Ichikawa, T. Hikage, S. Kakuta, and K. Nagai, *Chem. Phys. Lett.*, **549**, 77 (2012).
12. P. Arunachalam, S. Zhang, T. Abe, M. Komura, T. Iyoda, and K. Nagai, *Appl. Catal., B*, (2016).
13. S. Zhang, R. Sakai, T. Abe, T. Iyoda, and K. Nagai, *ACS Appl. Mater. Interfaces*, **3**, 1902 (2011).
14. K. Nagai, T. Abe, Y. Kaneyasu, Y. Yasuda, I. Kimishima, T. Iyoda, and H. Imaya, *ChemSusChem*, **4**, 727 (2011).
15. K. Nagai, Y. Yasuda, T. Iyoda, and T. Abe, *ACS Sustain. Chem. & Eng.*, **1**, 1033 (2013).
16. K. Nagai and T. Abe, *Kobunshi Ronbunshu*, **70**, 459 (2013).
17. T. Abe, K. Nagai, M. Kaneko, T. Okubo, K. Sekimoto, A. Tajiri, and T. Norimatsu, *ChemPhysChem*, **5**, 716 (2004).
18. S. Zhang, P. Arunachalam, T. Abe, T. Iyoda, and K. Nagai, *J. Photochem. Photobiol., A*, **244**, 18 (2012).
19. L. Steier, S. Bellani, H. C. Rojas, L. Pan, M. Laitinen, T. Sajavaara, F. Di Fonzo, M. Grätzel, M. R. Antognazza, and M. T. Mayer, *Sustainable Energy Fuels*, **1**, 1915 (2017).
20. T. Bourgeteau, D. Tondelier, B. Geffroy, R. Brisse, R. Cornut, V. Artero, and B. Jousselme, *ACS Appl. Mater. Interfaces*, **7**, 16395 (2015).
21. M. Hiramoto, H. Fujiwara, and M. Yokoyama, *Appl. Phys. Lett.*, **58**, 1062 (1991).
22. P. Peumans, S. Uchida, and S. R. Forrest, *Nature*, **425**, 158 (2003).
23. T. Kuwabara, H. Sugiyama, T. Yamaguchi, and K. Takahashi, *Thin Solid Films*, **517**, 3766 (2009).
24. T. Abe, K. Nagai, H. Ichinohe, T. Shibata, A. Tajiri, and T. Norimatsu, *J. Electroanal. Chem.*, **599**, 65 (2007).
25. T. Abe, H. Ichinohe, S. Kakuta, and K. Nagai, *Jpn. J. Appl. Phys.*, **49**, 015101 (2010).
26. T. Abe, S. Tobinai, and K. Nagai, *Jpn. J. Appl. Phys.*, **48**, 021503 (2009).
27. T. Abe, S. Miyakushi, K. Nagai, and T. Norimatsu, *Phys. Chem. Chem. Phys.*, **10**, 1562 (2008).
28. K. Nagai, T. Iyoda, A. Fujishima, and K. Hashimoto, *Solid State Commun.*, **102**, 809 (1997).
29. N. J. Turro, V. Ramamurthy, and J. C. Scaiano, *Principles of Molecular Photochemistry: An Introduction*, University Science Books, Sausalito, California, p. 248 (2010).
30. F. Piersimoni, D. Cheyns, K. Vandewal, J. V. Manca, and B. P. Rand, *J. Phys. Chem. Lett.*, **3**, 2064 (2012).
31. A. Guerrero, H. Heidari, T. S. Ripolles, A. Kovalenko, M. Pfannmöller, S. Bals, L. D. Kauffmann, J. Bisquert, and G. Garcia-Belmonte, *Adv. Energy Mater.*, **5**, 1401997 (2015).
32. K. Akaike, K. Kanai, Y. Ouchi, and K. Seki, *Adv. Funct. Mater.*, **20**, 715 (2010).
33. T. Maki and H. Hashimoto, *Bull. Chem. Soc. Jpn.*, **25**, 411 (1952).
34. K. Nagai, Y. Fujimoto, H. Shiroishi, M. Kaneko, T. Norimatsu, and T. Yamanaka, *Chem. Lett.*, **30**, 354 (2001).
35. T. Morikawa, C. Adachi, T. Testuo, and S. Saito, *Nippon Kagaku Kaishi*, **1990**, 962 (1990).
36. T. Abe, S. Ogasawara, K. Nagai, and T. Norimatsu, *Dyes Pigm.*, **77**, 437 (2008).
37. T. Abe and K. Nagai, *Org. Electron.*, **8**, 262 (2007).
38. O. V. Mikhnenko, P. W. M. Blom, and T. Q. Nguyen, *Energy Environ. Sci.*, **8**, 1867 (2015).
39. E. Karmann, D. Schlettwein, and N. I. Jaeger, *J. Electroanal. Chem.*, **405**, 149 (1996).